Weighing neutrinos using high redshift galaxy luminosity functions

Charles Jose[1],* Saumyadip Samui[2],† Kandaswamy Subramanian[1],‡ and Raghunathan Srianand[1§]
1. IUCAA, Pune University Campus, Ganeshkhind, Pune 411007, INDIA. and
2. SISSA, via Bonomea, 265, 34136 Trieste, Italy
(Dated: April 20, 2011)

Laboratory experiments measuring neutrino oscillations, indicate small mass differences between different mass eigenstates of neutrinos. The absolute mass scale is however not determined, with at present the strongest upper limits coming from astronomical observations rather than terrestrial experiments. The presence of massive neutrinos suppresses the growth of perturbations below a characteristic mass scale, thereby leading to a decreased abundance of collapsed dark matter halos. Here we show that this effect can significantly alter the predicted luminosity function (LF) of high redshift galaxies. In particular we demonstrate that a stringent constraint on the neutrino mass can be obtained using the well measured galaxy LF and our semi-analytic structure formation models. Combining the constraints from the Wilkinson Microwave Anisotropy Probe 7 year (WMAP7) data with the LF data at $z \sim 4$, we get a limit on the sum of the masses of 3 degenerate neutrinos $\Sigma m_\nu < 0.52$ eV at the 95 % CL. The additional constraints using the prior on Hubble constant strengthens this limit to $\Sigma m_\nu \leq 0.29$ eV at the 95 % CL. This neutrino mass limit is a factor ~ 4 improvement compared to the constraint based on the WMAP7 data alone, and as stringent as known limits based on other astronomical observations. As different astronomical measurements may suffer from different set of biases, the method presented here provides a complementary probe of Σm_ν. We suggest that repeating this exercise on well measured luminosity functions over different redshift ranges can provide independent and tighter constraints on Σm_ν.

PACS numbers: 98.80.Es, 14.60.Pq, 98.62.Ve, 95.80.+p

I. INTRODUCTION

A cosmic background of neutrinos is one of the key predictions of standard cosmology. Their predicted abundance is comparable to that of the relic photons. Thus if neutrinos have a mass they can contribute significantly to the matter density in the universe. Experiments which detect neutrino oscillations have measured small but non-zero differences between the mass eigenstates of neutrinos, with at least one of them having a mass larger than ~ 0.05 eV [1, 2]. The absolute mass scale of neutrinos could be inferred from various β-decay experiments [3, 4]. However at present stronger constraints on neutrino mass are obtained from cosmological observations. In particular observations related to anisotropies in the Cosmic Microwave Background Radiation (CMBR) and the growth of structure in the universe can play an important role (see [5, 6] for reviews). For example the recent WMAP7 data itself has been used to set an upper limit on the of sum of neutrino masses, $\Sigma m_\nu < 1.15 - 1.3$ eV, for sudden reionization [7, 8] and $\Sigma m_\nu < 1.7$ eV for a generalized reionization scenario [8]. Thus one is dealing with the universe having matter density dominated by cold dark matter (CDM) with massive neutrino (Hot dark matter, HDM) providing sub-dominant contribution (i.e the neutrino density parameter $\Omega_\nu = \Sigma m_\nu / 93.14 h^2 \text{eV} \leq 0.014 h^{-2}$, where h is the Hubble constant H_0 in units of 100 km s^{-1} Mpc^{-1}; see chapter 2 of Ref. [18]). This is usually referred to as the mixed dark matter (MDM) scenario.

Interestingly, the presence of even such a subdominant HDM component leads to the suppression of the growth of density perturbations below a scale known as the free streaming scale [9]. This suppression occurs because neutrinos escape (or free-stream out of) their own density perturbations below the free-streaming scale. Thus only the CDM component can lead to perturbation growth below this scale. This free streaming scale is time dependent and also depends on the neutrino mass. The suppression of the growth of density perturbations below the free streaming scale leads to a reduction in the matter power spectrum and a delay in the formation of structures in the universe. This in turn results in a reduced abundance of dark matter halos at any given epoch, above a characteristic mass scale. Thus observations related to large scale structure formation in the universe can be used to probe the absolute mass scale of neutrinos. It has been shown that sub eV constraints are obtained on neutrino mass by combining CMB data

*Electronic address: charles@iucaa.ernet.in
†Electronic address: ssamui@gmail.com
‡Electronic address: kandu@iucaa.ernet.in
§Electronic address: anand@iucaa.ernet.in

with currently available data on galaxy surveys at low redshift [10], counts of low redshift massive galaxy clusters [11], inter-galactic medium (IGM) Lyman-α absorption power spectrum [12, 13] and weak lensing [14]. Unlike CMB observations all the astrophysical observations are affected by different systematics related to baryonic physics. Thus it is important to explore whole range of observables (with different biases) to get realistic constraints on Σm_ν. There is a growing wealth of observations on high redshift galaxies which may also provide independent and equally useful constraints on neutrino mass. Thus in this work we explore the possibility of using the luminosity functions (LF) of high redshift Lyman break galaxies (LBGs) for constraining Σm_ν.

The basic idea is as follows: The reduction in the matter power spectrum in models with $\Sigma m_\nu > 0$, compared to models where $\Sigma m_\nu = 0$ implies a reduced abundance of galactic scale dark matter halos at high redshifts. In order to account for the observed LF of these galaxies (in number per unit volume per unit luminosity), the light to mass ratio of each galactic halo has to be systematically higher in the models with $\Sigma m_\nu > 0$. However changing the light to mass ratio is degenerate with the unknown extinction correction one applies to the observed LF. Nevertheless, this degeneracy can be lifted if one has a feature in the LF at some characteristic mass scale, introduced by various feedback processes like the radiative feedback after reionization. In such cases the shape of the predicted galaxy luminosity function depends on the neutrino mass. We use this idea to constrain neutrino mass. In the next section we discuss structure formation models incorporating massive neutrinos. Section III describes our semi-analytic models for the UV luminosity functions. The effect of a non-zero neutrino mass on the high redshift LFs is studied in Section IV. We present our limits on Σm_ν in Section V using a Markov Chain Monte Carlo analysis and conclude in Section VI.

II. STRUCTURE FORMATION IN MDM COSMOLOGY

A crucial ingredient of any model of structure formation is $\sigma(M, z)$, the rms density fluctuations on any mass scale M as a function of redshift z. This is given by

$$\sigma^2(M, z) = \sigma^2(R, z) = \int_0^\infty \frac{dk}{2\pi^2} k^2 P_k(z) W^2(k, R) \tag{1}$$

where R is the comoving radius of a sphere containing mass M, k is the comoving wave number, $W(k, R)$ is the top hat window function in Fourier space and $P_k(z)$ is the linear power spectrum of the density fluctuations at z. For a universe with massive neutrinos $P_k(z) = T^2(k, z, z_i; m_\nu) P_k(z_i)$. Here $P_k(z_i)$ is the initial power spectrum at z_i and the function $T(k, z, z_i; m_\nu)$ is the matter transfer function in a ΛCDM universe with massive neutrinos.

The transfer function in mixed dark matter (MDM) cosmology with neutrinos has been studied extensively [9, 15, 16]. Eisenstein and Hu [16] give a fitting formula of the form

$$T(k, z, z_i; m_\nu) = T_{master}(k; m_\nu) D(k, z, z_i; m_\nu). \tag{2}$$

The function $D(k, z, z_i; m_\nu)$ is the scale dependent growth factor of CDM, baryon and neutrino perturbations in a ΛCDM universe in presence of free streaming neutrinos and T_{master} is a master-transfer function. The explicit forms of both these functions are given by Eisenstein and Hu [16] (see also [15]). Their fit is optimized for a total number of three neutrinos which include massive as well as massless species. Note that the standard model of particle physics predicts the effective number of neutrinos (N_ν) to be 3.04 with the 0.04 coming from incomplete neutrino freeze-out and finite temperature effects around e^+ e^- annihilation [6]. We have checked that this transfer function is in good agreement with T computed numerically using the 'CAMB' code [19] (Lewis, Challinor & Lasenby 2000). We will also fix $N_\nu = 3$ and adopt this transfer function while calculating the luminosity functions below.

Given the transfer function and $\sigma(M, z)$ one can estimate the abundance of dark matter halos, for example using the Press-Schechter (PS) [20] approach. This also requires one to specify δ_c, the linearly extrapolated critical density contrast needed for collapse of a spherical top hat over dense region. For a flat universe with only CDM, the critical density contrast of collapse is 1.686 [21, 22]. The calculation of δ_c for the ΛCDM model without any massive neutrino species, has been done before by [23], who found that δ_c for this model is very nearly the same as that for the pure CDM model. However, to our knowledge, a corresponding estimate of δ_c does not exist for models with massive neutrinos. As the abundance of halos is exponentially sensitive to the value of δ_c when using the PS formalism, it is important to estimate it even in MDM models. We do this below using the spherical model for nonlinear evolution adopting a flat ΛCDM universe with massive neutrinos.

A. Spherical model for nonlinear collapse in MDM cosmology

The spherical model or top hat model [24], gives the nonlinear growth of a uniformly overdense spherical region in a smooth background of expanding universe. In spherical model we study the evolution of physical density contrast

$\delta(r,z)$ in real space directly rather than the evolution of it's Fourier components $\delta(k,z)$. For this purpose, we assume a spherical uniformly over dense region in the background expanding universe. Below the free-streaming scale of the neutrinos, only the CDM and baryons can cluster due to gravity, although both the cosmological constant Λ and neutrinos will contribute to the expansion. Note that the mass associated with the free streaming scale is much larger than the galactic scales we consider below. Thus the clustering mass is solely contributed by the baryons and the CDM. This is also borne out by recent simulations of structure formation in an MDM universe by Brandbyge et al [25].

The gravitational acceleration of the shell of radius r (with initial radius r_i) in the spherical model is then given by

$$\ddot{r} = -\frac{GM(z_i)}{r^2} - \frac{4}{3}\pi G(\rho_\nu(z) - 2\rho_\Lambda)r. \tag{3}$$

Here M is the total mass which can cluster within the spherical region, and hence does not include any contribution from the neutrinos. Explicitly we have

$$M = 4\pi r_i^3(\rho_{CDM}(z_i) + \rho_b(z_i))(1+\delta_{cb}(z_i))/3 = 4\pi r_i^3(1-f_\nu)\rho_m(z_i)(1+\delta_{cb}(z_i))/3. \tag{4}$$

Here $\rho_{CDM}(z)$, $\rho_b(z)$, $\rho_\nu(z)$ and $\rho_\Lambda(z)$ are respectively the background densities of CDM, baryons, neutrinos and cosmological constant at redshift z. We have also defined the neutrino fraction $f_\nu = \rho_\nu/\rho_m$, with $\rho_m = \rho_{CDM}+\rho_b+\rho_\nu$ is the total matter density. Further $\delta_{cb} = (\delta\rho_{CDM}+\delta\rho_b)/(\rho_{CDM}+\rho_b)$ is fractional overdensity in the CDM + baryon component within the spherical region. Note that the total density contrast $\delta_m = \delta\rho_m/\rho_m = \delta_{cb}(1-f_\nu)$, since $\delta\rho_\nu = 0$ inside the spherical region. Even though neutrinos do not cluster below their free-streaming scale, their uniform density does lead to a deceleration of the shell, through the $\rho_\nu(z)$ term in Eq. (3). Moreover the cosmological constant leads to a positive acceleration of the shell proportional to $(\rho_\Lambda + 3p_\Lambda)$, where the pressure $p_\Lambda = -\rho_\Lambda$. At any redshift z and $\rho_\Lambda(z) = \rho_c\Omega_\Lambda(0)$ and $\rho_\nu(z) = \rho_c\Omega_\nu(1+z)^3$, where Ω_i is the present density of component 'i' in units of the critical density ρ_c.

The Hubble expansion rate at any redshift is given by

$$H(z) = H(0)\left(\Omega_m(1+z)^3 + \Omega_\Lambda\right)^{1/2} \tag{5}$$

where $H(0)$ is the present value of Hubble constant. Noting that

$$dt = \frac{dt}{da}\frac{da}{dz}dz = -\frac{dz}{H(z)(1+z)^3}, \tag{6}$$

we can numerically solve Eqn. (3) for a given set of initial conditions to obtain trajectory of the shell $r(z)$, and the redshift of collapse z_c. We assume that initially the density contrast $\delta_{cb}(z_i) = \delta_i$ is small enough that the overdense region is expanding along with the background. Thus the initial velocity of the shell at radius r is $v_i = H(z_i)r(z_i)$.

Once we know the redshift of collapse z_c, we can evolve linear equations of perturbations using the same initial conditions to calculate the linearly extrapolated critical density contrast, δ_c at z_c. This linear evolution of δ_{cb} for scales much below the free streaming scale is governed by

$$\ddot{\delta}_{cb} + 2H\dot{\delta}_{cb} - 4\pi G(1-f_\nu)\Omega_m\rho_c\delta_{cb} = 0, \tag{7}$$

whose solution can only be determined numerically for a Λ+MDM universe.

In the upper panel of Fig. 1, we give δ_c for $z_c = 0$ as a function of Ω_Λ, as determined by the above procedure, assuming zero mass for the neutrinos. We confirm the weak dependence of δ_c on Ω_Λ (with δ_c differing from 1.686 only by 0.5% for $\Omega_\Lambda = 0.7$), as also found by [23]. Note that even smaller changes in δ_c ($\sim 0.006\%$) would obtain in a ΛCDM model for the higher collapse redshifts (say $z_c = 4$) relevant for our work. In the middle panel of Fig. 1, we show the δ_c dependence on Σm_ν, for $z_c = 4$. We have adopted the cosmological parameters of a fiducial model with $\Omega_\Lambda = 0.735$ and $h = 0.71$. The change in δ_c is very small even in the case of universe with massive neutrinos for the Σm_ν range constrained by CMBR observations. For example, with $z_c = 4$, δ_c decreases only to 1.68 for $\Sigma m_\nu = 1$ eV, or only a decrease of $\sim 0.4\%$ from the canonical value. The bottom panel gives δ_c as a function of z_c for $\Sigma m_\nu = 1$ eV and for the cosmological parameters as above. At $z_c \sim 0$ now δ_c decreases to 1.671 (or a fractional change of $\sim 0.9\%$), due to the additional effect of the Ω_Λ at such low redshifts. Based on the above discussion, it is a reasonable approximation to take the fiducial value of $\delta_c = 1.686$, when computing the abundance of halos at high redshifts, even in the presence of massive neutrinos.

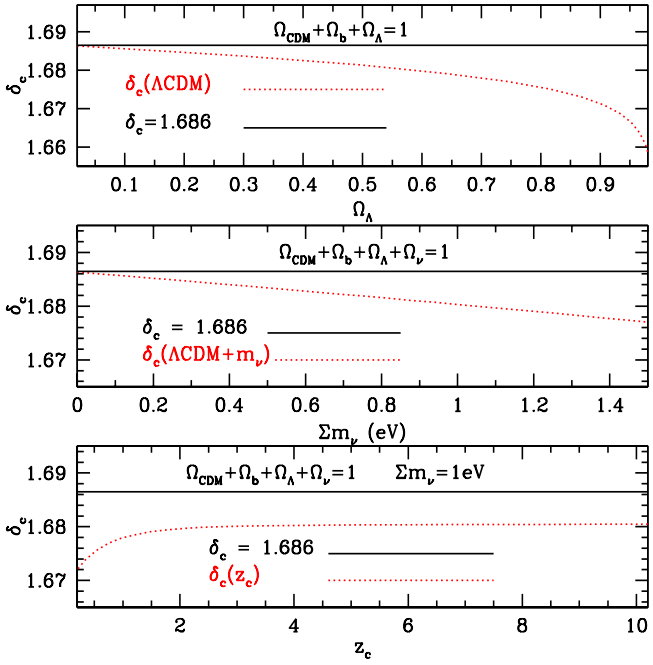

FIG. 1: Dependence of δ_c on various parameters. The top panel shows δ_c as a function of Ω_Λ for a ΛCDM universe without any massive neutrinos, with $z_c = 0$. The middle panel shows δ_c as a function of Σm_ν for ΛCDM universe with massive neutrinos where $z_c = 4$. The cosmological parameters are chosen according to our fiducial model ($\Omega_\Lambda = 0.735$, $h = 0.71$) and by keeping $\Omega_{CDM} + \Omega_b + \Omega_\nu = 0.265$. In the bottom panel the dependence of δ_c on z_c is plotted for $\Sigma m_\nu = 1$ eV and for the cosmological parameters as above. In all the panels the solid horizontal (solid dark) line at 1.686 corresponds to δ_c for a universe with only CDM in it. The red dotted line shows the variation in δ_c with the parameter of interest.

B. The abundance of halos

The abundance of dark matter halos as a function of mass and redshift plays a crucial role in understanding various aspects of galaxy formation. This halo mass function can be obtained through analytical formulations as well as N-body simulations. The first analytical form of halo mass function was given by Press and Schecter [20]. Subsequently several alternative mass functions have been suggested which better fit the results of N-body simulations, a popular choice being the Sheth-Tormen (ST) mass function [27]. These mass functions assume the initial density field to be Gaussian random. And also that a region of size R (containing a mass M) collapses when its linearly extrapolated density contrast reaches a critical density δ_c, as predicted by the spherical model of nonlinear evolution. We found above that δ_c for the CDM+baryon component is only slightly altered from the canonical value of 1.686, by the presence of massive neutrinos.

Brandbyge et al [25] have shown that the ST mass function provides an excellent fit for mass functions of dark matter halos obtained from N-body simulations including massive neutrinos. This has also been confirmed recently by Marulli et al [26]. In the ST formula the comoving number density of halos with mass between M and M+dM at any redshift z is given by

$$N_{ST}(M,z)dM = \frac{\rho}{M} A \sqrt{\frac{2a}{\pi}} \left[1 + \left(\frac{\sigma^2}{a\delta_c^2}\right)^p\right] \frac{\delta_c}{\sigma} \left(\frac{-1}{\sigma}\frac{d\sigma}{dM}\right) \exp\left(\frac{-a\delta_c^2}{2\sigma^2}\right) dM \tag{8}$$

where from the numerical fitting $A = 0.3222$, $a = 0.707$, $p = 0.3$ and $\delta_c = 1.686$. Brandbyge et al [25] also find that one needs to use $\rho = \rho_{cb} = (\rho_{CDM} + \rho_b)$ and calculate the mass as $M = M_{cb} = 4\pi r^3(\rho_{CDM} + \rho_b)/3$ in using ST formula to fit the halo abundance. However they calculate σ using the total matter power spectrum [25] (also Brandbyge; private communication), although naively one may have expected that σ should be calculated using the

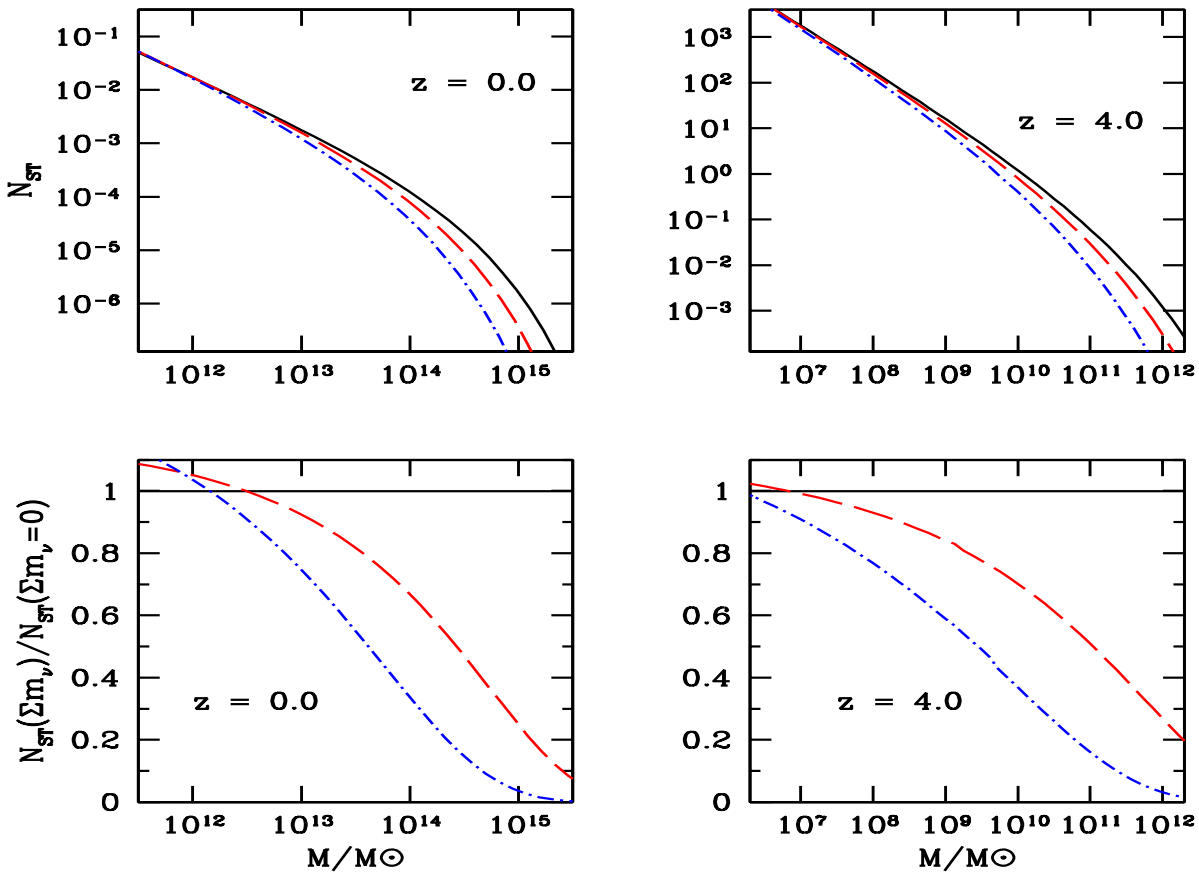

FIG. 2: The halo abundance N_{ST} for ΛCDM and ΛMDM models. The top panels show N_{ST} as a function of halo mass for $\Sigma m_\nu = 0$ (solid black lines), $\Sigma m_\nu = 0.5$ eV (long dashed red lines) and $\Sigma m_\nu = 1$ eV (dash-dotted blue lines). The bottom panels show the ratio of N_{ST} for different values of Σm_ν to that obtained taking $\Sigma m_\nu = 0$. The left panels are for $z = 0$, while the right panels are for $z = 4$.

power spectrum of CDM+baryons [1]. In our work we follow the prescription of [25] in calculating the halo abundance, as this seems to fit the simulated data well.

We illustrate the effect of massive neutrinos on the abundance of dark matter halos in Fig. 2, where we plot in the upper panels, N_{ST}, using the prescription of [25], for two redshifts $z = 0$ and $z = 4$. The solid black line in Fig. 2 gives N_{ST}, for a fiducial ΛCDM model with $\Sigma m_\nu = 0$. As the fiducial ΛCDM model, we adopt a set cosmological parameters consistent with WMAP-CMBR 7 year data [28]. Thus we adopt $h = 0.71$, $\Omega_b = 0.0448$ and $\Omega_{CDM} = 0.220$. The initial power spectrum is specified by the best fit values of scalar spectral index $n_s = 0.953$ and curvature fluctuation amplitude $\Delta^2_R = 2.43 \times 10^{-9}$ at a pivot scale $k_0 = 0.002 Mpc^{-1}$ (or a $\sigma_8 = 0.801$). We then examine models with non-zero Σm_ν by varying Ω_{CDM} and satisfying the constraint that $\Omega_{CDM} + \Omega_\nu = 0.220$. The long dashed (red) line gives N_{ST} for the case when $\Sigma m_\nu = 0.5$ eV, while the dash-dotted (blue) line is for the case $\Sigma m_\nu = 1$ eV. The bottom panels give the ratio of N_{ST} between the non-zero neutrino mass cases with respect to the fiducial model, as a function of M.

From this figure we can see that the number of collapsed halos decreases with increase in neutrino mass for halo mass scales above a characteristic mass scale M_c, while there is a slight increase in abundance of halos below this mass scale. The characteristic mass $M_c \sim 10^{12} M_\odot$ at $z = 0$ while $M_c \sim 1.6 \times 10^6 M_\odot$ at $z = 4$ for $m_\nu = 1$ eV.

[1] Note that, for length scales much smaller than the free-streaming scale, since $\delta_m = \delta_{cb}(1 - f_\nu)$, σ calculated from the total matter power spectrum is $\approx \sigma_{cb}(1 - f_\nu)$, where σ_{cb} is that calculated from the power spectrum of the CDM+baryons.

The decrease in abundance of large mass halos arises as a result of the suppression of growth due to the presence of free-streaming neutrinos. In our model with $\Sigma m_\nu = 1.0$ eV, we find that at $z = 0$, the abundance of galaxy clusters of mass $M \sim 10^{14} M_\odot$ decreases by a factor ~ 3.2, while for bigger clusters with $M \sim 10^{15} M\odot$, the decrease in abundance is by a factor ~ 25. Similarly at $z = 4$, the abundance of galactic scale halos of mass $10^{11} M_\odot$ and $10^{12} M_\odot$ are suppressed respectively by factors ~ 6.5 and ~ 30, in models with $\Sigma m_\nu = 1$eV compared to the zero neutrino mass case. Thus strong constraints on the neutrino mass can be obtained from measuring the abundance of galaxy clusters at low redshifts or equally, the abundance of galaxies at high redshifts as probed by their observed luminosity functions.

III. HIGH REDSHIFT GALAXY LUMINOSITY FUNCTIONS

In the previous section we have described how the presence of massive neutrinos suppresses the high redshift galactic halo formation. In this section, using semi-analytical models, we investigate the effect of massive neutrinos on high redshift galaxy UV LF. We model high redshift galaxy LF using the semi-analytical treatment of Samui, Srianand & Subramanian (2007) [31] (hereafter SSS07) which were successful in explaining the observed luminosity functions at $3 \leq z \leq 10$. (see also Samui, Subramanian & Srianand (2009) [30]; hereafter SSS09). Here, we use the same approach in order to constrain neutrino masses. We briefly describe the modeling here and the interested reader may refer to SSS07 and SSS09 for more details.

The star formation rate of an individual dark matter halo of mass M collapsed at redshift z_c and observed at redshift z is modeled by (see [32], [33])

$$\dot{M}_{SF}(M, z, z_c) = f_* \left(\frac{\Omega_b}{\Omega_m} M \right) \frac{t(z) - t(z_c)}{\kappa^2 t^2_{dyn(z_c)}} \times \exp \left[- \frac{t(z) - t(z_c)}{\kappa t_{dyn(z_c)}} \right], \tag{9}$$

where f_* is the fraction of the total baryonic mass that is converted into stars over the entire lifetime of the galaxy. Here $t_{dyn}(z_c)$ is the dynamical time scale of a halo collapsing at z_c (Eq. (3) of SSS07) and κ is a parameter which governs the duration of the star formation activity in the halo which we take here to be unity. Further, $t(z)$ is the age of the universe at redshift z; thus $t(z) - t(z_c)$ is the age of the galaxy at z. We assume that stars are formed with a normal Salpeter IMF in the mass range from $1 - 100\ M_\odot$. The population synthesis code Starburst99 [34] is used to obtain the luminosity of a galaxy undergoing a burst of star formation, as a function of time for a given rest wavelength of 1500 Å. The assumed star formation rate of a galaxy in Eq. (9) is then convolved with this burst luminosity to get the evolution of luminosity (L_{1500}) of an individual star forming galactic halo (See Eq. (6) and figure 1 of SSS07). Only a fraction $(1/\eta)$ of the total light produced by the stars comes out of the galaxy due to the absorption by dust. We convert this luminosity ($L = L_{1500}/\eta$) to a standard absolute AB magnitude M_{AB} using the equation given by [35]. The luminosity function $\Phi(M_{AB}, z)$ at any redshift z is then given by [31]

$$\Phi(M_{AB}, z)\ \mathrm{d}M_{AB} = \int_z^\infty \mathrm{d}z_c\ \frac{\mathrm{d}N_{ST}(M, z_c)}{\mathrm{d}z_c} \quad \frac{\mathrm{d}M}{\mathrm{d}L_{1500}}\ \frac{\mathrm{d}L_{1500}}{\mathrm{d}M_{AB}}\ \mathrm{d}M_{AB} \tag{10}$$

where $\mathrm{d}N_{ST}(M, z_c)/\mathrm{d}z_c = \dot{N}_{ST}(M, z_c)dt/dz_c$, and $\dot{N}_{ST}(M, z_c)dM$ is the formation rate of objects in the mass range $(M, M + dM)$ at redshift z_c. We model this formation rate as the time derivative of ST mass function as (i) they are found to be the best in reproducing the observed LF of high-z LBGs (see SSS09), and (ii) as explained earlier gives good fit to the abundance of dark matter halos in N-body simulations incorporating massive neutrinos [25].

Star formation in a given halo also depends on the cooling efficiency of the gas and various feedback processes. We assume that gas in halos with virial temperatures (T_{vir}) in excess of 10^4 K can cool (due to recombination line cooling from hydrogen and helium) and collapse to form stars. However the ionization of the IGM by UV photons increases the temperature of the gas thereby increasing the Jean's mass for collapse. Thus in ionized regions, we incorporate this feedback by a complete suppression of star formation for halos with circular velocity $v_c \leqslant 35$ km s^{-1} and no suppression with $v_c \geqslant V_u = 95$ km s^{-1} [36]. For intermediate circular velocities, a linear fit from 1 to 0 is adopted as the suppression factor ([36]; see also [37, 38], SSS07). In SSS07 we found that this feedback mechanism naturally leads to the observed flattening of the LF at the low luminosity end [2]. Note that implementing radiative feedback in

[2] In principle, one could also consider star formation in smaller mass halos with $T_{\rm vir} \geq 300$ K, where the cooling is due to the H_2 molecular line emission [39]. While star formation in such halos could be important for reionization and IGM metal enrichment, in the post reionization era, it is suppressed by radiative feedback.

	$\Sigma m_\nu = 0$ eV			$\Sigma m_\nu = 0.5$ eV			$\Sigma m_\nu = 1$ eV		
z	f_*/η	χ^2	χ^2_ν	f_*/η	χ^2	χ^2_ν	f_*/η	χ^2	χ^2_ν
3.0	0.040	15.14	1.89	0.052	19.42	2.16	0.086	31.39	3.92
4.0	0.039	16.09	1.46	0.067	19.49	1.77	0.152	40.08	3.46
5.0	0.030	45.71	5.07	0.054	44.87	4.99	0.179	12.91	1.43
6.0	0.041	4.34	0.72	0.082	5.64	0.94	0.250	4.97	0.83

TABLE I: The best fit values f_*/η, corresponding χ^2 and reduced χ^2_ν for our models at various redshifts for three different values of Σm_ν.

a model requires a knowledge of the reionization epoch. A number of observations suggest that reionization is nearly complete by a redshift $z_{re} \geq 6$ (e.g. [7, 43]). We will show below that the strongest constraints on neutrino masses are obtained from the luminosity function at $z = 4$. As this redshift is much lower than z_{re}, our limits on the neutrino mass then turns out to be insensitive to the exact z_{re} as long as it is greater than 6.

In our models, we also incorporate the possible Active Galactic Nuclei (AGN) feedback that suppresses star formation in the high mass, by multiplying the star formation rate by a factor $[1 + (M/M_{AGN})^3]^{-1}$, as in SSS07. This sharply decreases the star formation activity in high mass halos above a characteristic mass scale M_{AGN}, which is believed to be $\sim 10^{12} M_\odot$ (see [40, 42]). The determination of M_{AGN} is done by fitting luminosity functions at a fiducial redshift and will be discussed below. In what follows, we compute the high redshift luminosity functions of galaxies in the presence of massive neutrinos using the above semi-analytical prescription and comparing it with observations to put limits on neutrino mass.

IV. EFFECT OF NEUTRINO MASS ON HIGH REDSHIFT LF

We now illustrate the effect of massive neutrinos on high redshift galaxy UV LF. We show in Fig. 3 our model predictions of luminosity functions at different redshifts, $z = 3 - 6$, along with the observational data. The redshifts are indicated at the top of each panel. The observed data points are taken from Reddy et. al (2007) [41] for $z = 3$, and Bouwens et. al. (2007) [45] for $z = 4,\ 5$ and 6, and corrected to the fiducial WMAP7 cosmology described earlier. As in SSS09, we take into account cosmic variance ([44]; [45]) and add an uncertainty of 14% to the Poisson error in quadrature for redshift $4 - 6$ data.

The solid line shows the predicted best fit luminosity functions at various redshifts for the fiducial cosmology and with $\Sigma m_\nu = 0$. In order to fit the observed data points we have adjusted the free parameter f_*/η in our models, using χ^2 minimization. We use all the points excluding the last two data points for $z = 4, 5$ and the last point for $z = 6$, in the low luminosity end while fitting the LF, as these points are affected by the incompleteness of the survey (see [45]). For this illustrative study, we also fix $V_u = 95$ km s^{-1} and adopt $M_{AGN} = 1.8 \times 10^{12} M_\odot$ that best fits the LF at $z = 4$ with $\Sigma m_\nu = 0$.

Our model with $\Sigma m_\nu = 0$ (solid curve) reproduces the observed LF very well at all the redshifts except $z = 5$ (where SSS09 also earlier pointed out one discrepant point). The best fit values of f_*/η at different redshifts and the corresponding χ^2 and reduced χ^2_ν, are tabulated in Table I. The required values of f_*/η, and reduced χ^2_ν, at different z are nearly the same and similar to what we obtained in SSS09 (which used slightly different cosmological parameters). The flattening of the predicted LF as seen in Fig. 3 at the faint end is due to the radiative feedback.

The thick dashed-dotted (blue) curves show the predicted LF if we use the same f_*/η for a MDM model with $\Sigma m_\nu = 1.0$ eV. It is clear that there is an order of magnitude suppression in the number density of galaxies at a given luminosity, which increases with increasing redshift. This is because the presence of neutrinos suppresses the formation rate of halos at the mass and redshift scales of our interest. We can make our model predictions match with the observed data by increasing f_*/η (i.e shifting this curve along the luminosity axis). These best fit values of f_*/η at different redshifts for the case $\Sigma m_\nu = 1$ eV, and the corresponding reduced χ^2_ν, are also tabulated in Table I. Firstly, we can see from Table I, that at each z the value of f_*/η (or light to mass ratio) needed to fit the observed luminosity function increases with Σm_ν. For example, at $z = 6$ one needs ~ 6 times more baryons to convert into stars for a model with $\Sigma m_\nu = 1$ eV compared to the zero neutrino mass case. Furthermore, for $\Sigma m_\nu = 1$ eV, the value of f_*/η required to fit the UV LFs also increases significantly with z, in contrast to the zero neutrino mass case. Therefore, any independent constraint on f_*/η, especially at high z, could lead to useful constraints on the neutrino

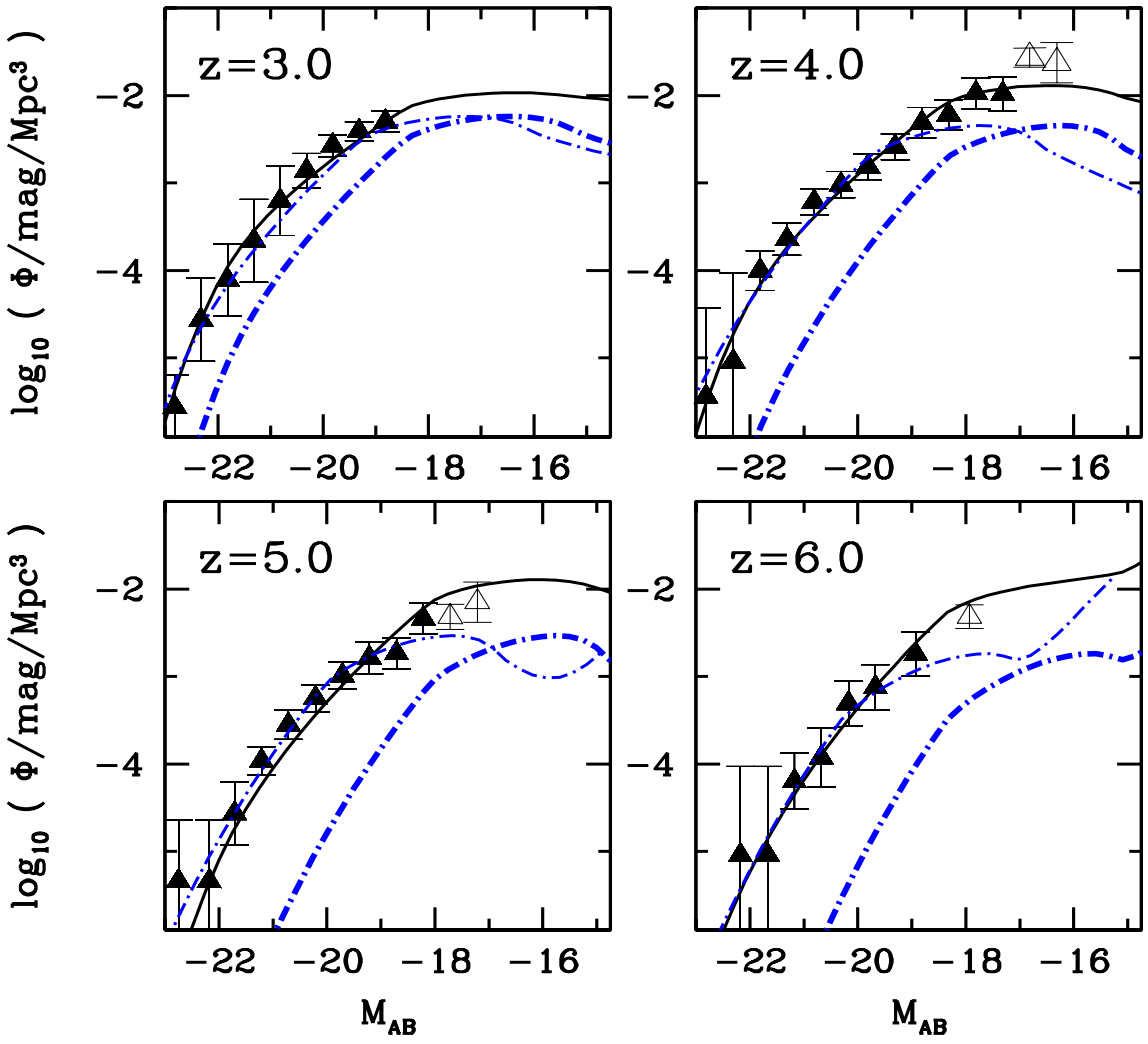

FIG. 3: UV LF of LBGs at redshifts $3, 4, 5$ and 6. The solid (black) line shows the predicted best fit LF for our model with $\Sigma m_\nu = 0$. The thick dashed-dotted (blue) curve shows our model predictions with $\Sigma m_\nu = 1$ eV and using the same best fit f_*/η as the $\Sigma m_\nu = 0$ eV model. This is to illustrate the suppression due to massive neutrinos. The thin dashed-dotted (blue) curves are best fits for the models with $\Sigma m_\nu = 1$ eV. The data points (filled and open triangles) for $z = 3$ are taken from [41] and for $z = 4 - 6$ are from [45].

mass.

More importantly, these best fit luminosity functions, obtained with the new f_*/η (thin dashed-dotted curves), have a very different shape compared to the zero neutrino mass case. In particular, the predicted luminosity functions in models with $\Sigma m_\nu = 1$ eV, are suppressed at the low luminosity end compared to the zero mass case. This is basically because increasing f_*/η increases the light to mass ratio, which brings even small mass galaxies whose star formation has been suppressed due to radiative feedback, into the observable luminosity range. Therefore strong constraints on the neutrino mass can in principle be obtained by comparing the shape of the predicted luminosity functions with observations, independent of the free parameter f_*/η, provided the observations cover a wide luminosity range and in particular extend to the very faint end of the LF.

This requirement is at present best satisfied at $z = 4$. This is because, the observed LF for $z = 4$ is well defined over a wide range of luminosity thanks to the Hubble Ultra deep field (HUDF) and the Great Observatories Origins Deep Survey (GOODS) ([44, 45]). This redshift is also well below the redshift of reionization [7, 43]; so radiative feedback can be applied without any ambiguity. Therefore for demonstrating that quantitative limits on Σm_ν can be

Parameter	WMAP7	WMAP7 +LF	WMAP7 +HST	WMAP7 +LF +HST	WMAP7 (m_ν)	WMAP7 +LF (m_ν)	WMAP7 +LF +HST (m_ν)	WMAP7 +LF(FB)	WMAP7 LF(FB) +HST
$10^2\Omega_b h^2$	$2.223^{+0.060}_{-0.058}$	$2.229^{+0.055}_{-0.056}$	$2.263^{+0.050}_{-0.056}$	$2.259^{+0.054}_{-0.054}$	$2.245^{+0.060}_{-0.059}$	$2.229^{+0.055}_{-0.056}$	$2.257^{+0.053}_{-0.053}$	$2.235^{+0.056}_{-0.055}$	$2.266^{+0.051}_{-0.052}$
$10\Omega_{DM}h^2$	$1.172^{+0.070}_{-0.068}$	$1.228^{+0.065}_{-0.064}$	$1.107^{+0.051}_{-0.050}$	$1.169^{+0.056}_{-0.058}$	$1.177^{+0.071}_{-0.069}$	$1.235^{+0.065}_{-0.064}$	$1.168^{+0.056}_{-0.058}$	$1.208^{+0.060}_{-0.059}$	$1.156^{+0.045}_{-0.045}$
τ	$0.087^{+0.014}_{-0.014}$	$0.090^{+0.013}_{-0.014}$	$0.091^{+0.015}_{-0.015}$	$0.095^{+0.015}_{-0.014}$	$0.086^{+0.014}_{-0.014}$	$0.090^{+0.013}_{-0.014}$	$0.095^{+0.015}_{-0.014}$	$0.090^{+0.013}_{-0.014}$	$0.093^{+0.014}_{-0.015}$
n_s	$0.962^{+0.016}_{-0.015}$	$0.961^{+0.015}_{-0.014}$	$0.973^{+0.013}_{-0.013}$	$0.969^{+0.014}_{-0.016}$	$0.962^{+0.015}_{-0.015}$	$0.961^{+0.015}_{-0.014}$	$0.970^{+0.014}_{-0.016}$	$0.963^{+0.014}_{-0.014}$	$0.971^{+0.013}_{-0.012}$
σ_8	$0.717^{+0.071}_{-0.072}$	$0.820^{+0.051}_{-0.052}$	$0.756^{+0.049}_{-0.047}$	$0.821^{+0.042}_{-0.041}$	$0.717^{+0.071}_{-0.072}$	$0.824^{+0.051}_{-0.050}$	$0.821^{+0.042}_{-0.043}$	$0.808^{+0.038}_{-0.038}$	$0.813^{+0.030}_{-0.029}$
H_0	$66.1^{+4.1}_{-4.9}$	$65.5^{+2.8}_{-2.8}$	$70.3^{+2.5}_{-2.5}$	$68.7^{+2.1}_{-2.2}$	$66.0^{+4.2}_{-4.0}$	$65.3^{+2.9}_{-2.8}$	$68.7^{+2.2}_{-2.2}$	$66.3^{+2.9}_{-2.9}$	$69.2^{+2.2}_{-2.2}$
f_*/η	—	$0.035^{+0.007}_{-0.007}$	—	$0.036^{+0.007}_{-0.007}$	—	$0.034^{+0.005}_{-0.006}$	$0.035^{+0.007}_{-0.006}$	$0.037^{+0.005}_{-0.005}$	$0.037^{+0.005}_{-0.005}$
$\bar{f}_\nu$	< 0.091	< 0.048	< 0.052	< 0.028	—	—	—	< 0.042	< 0.026
Σm_ν(eV)	< 1.0	< 0.55	< 0.54	< 0.31	< 1.08	< 0.52	< 0.29	< 0.48	< 0.28

TABLE II: Results of our MCMC analysis to constrain Σm_ν. The first column lists the set of parameters that are obtained from our MCMC analysis. The last two rows give limits on $\bar{f}_\nu$ or Σm_ν, at the 95% CL. For cases where we constrain $\bar{f}_\nu$, the neutrino mass is given by $\Sigma m_\nu = 93.14\bar{f}_\nu\Omega_{DM}h^2$, where for $\Omega_{DM}h^2$ we use the mean value given in row 3. For other parameters their mean values and 1σ range are given.

obtained with well defined LF, we will concentrate below on the LF of LBGs at $z = 4$.

At this redshift we already see from Table I that, while $\chi^2 = 16.09$ for $\Sigma m_\nu = 0$ eV model, it increases by $\Delta\chi^2 \sim 3.4$ for $\Sigma m_\nu = 0.5$ eV and by $\Delta\chi^2 \sim 24$ for $\Sigma m_\nu = 1$ eV models. This suggests that $\Sigma m_\nu \sim 1$ eV is strongly disfavored at a 5σ level, and a typical 2σ upper limit is close to $\Sigma m_\nu \sim 0.5$ eV. While this is encouraging, we have been using a fixed set of cosmological parameters and therefore one needs to check if such a conclusion also follows when we vary these parameters. We examine this issue further below.

V. LIMITS ON NEUTRINO MASS

In the previous section we adopted a fiducial cosmology to examine the effect of a non-zero neutrino mass on the LF of LBGs. In order to obtain quantitative upper limits by exploring the full range of cosmological parameters consistent with both the WMAP7 data and the observed LF of LBGs, we have performed a Markov Chain Monte Carlo (MCMC) analysis using the publically available CosmoMC code [46] (we use the CosmoMC May 2010 version and the WMAP likelyhood code version 4.1). The default version of CosmoMC constrains the neutrino fraction in dark matter defined as $\bar{f}_\nu = \Omega_\nu/\Omega_{DM}$ where $\Omega_{DM} = \Omega_{CDM} + \Omega_\nu$. So we constrain $\bar{f}_\nu$ and obtain neutrino mass as $\Sigma m_\nu = 93.14\bar{f}_\nu\Omega_{DM}h^2$, where we use the mean value of Ω_{DM} from our MCMC analysis. We will also carry out the MCMC analysis by giving a prior in terms of Σm_ν to directly constrain its value. In addition to $\bar{f}_\nu$ (or Σm_ν), we explored the usual 7 dimensional parameter space $(\Omega_b h^2, \Omega_c h^2, \theta_s, \tau, n_s, A_s, A_{SZ})$.

In order to combine the constraints from the UV LF data with other constraints (like the WMAP7 data), we have added a new module to CosmoMC. This module computes the likelihood for LF of LBGs by comparing the theoretically predicted LF for any set of cosmological parameters with observed LF. The observed data points at $z = 4$ by [45], are for a cosmology with $\Omega_m = 0.3$ and $\Omega_\Lambda = 0.7$ and $h = 0.7$. Therefore for each set of cosmological parameters in the chain, we first correct the observed data to that cosmology, by modifying the volume and distance scales appropriately. Then for each member of the chain we compute the theoretical LF, compare it with the observed data, and minimize the χ^2 by varying f_*/η. This minimum χ^2 is used for calculating the LF likelihood.

We give the constraints on Σm_ν obtained from the MCMC analysis in Table II and Fig 5. The convergence of MCMC chains were diagnosed using the usual Gelman-Rubin statistic and an $R - 1 < 0.01$ was achieved in general. First we have examined the constraints from WMAP7 data alone [7, 47]. In this case we obtain an upper limit $\bar{f}_\nu < 0.091$ at the 95% CL, which when converted to a mass limit as described above, gives $\Sigma m_\nu < 1.0$ eV. The other cosmological parameters, given in column 2 of Table II, are almost identical to that obtained by [8] for their case of sudden reionization. Note that constraining Σm_ν directly gives a very similar limit $\Sigma m_\nu < 1.08$ eV at 95% CL with almost the same values for the other cosmological parameters (see column 6 of Table II).

Combining the UV luminosity function data at $z = 4$ with the WMAP7 data gives a significantly lower limit on

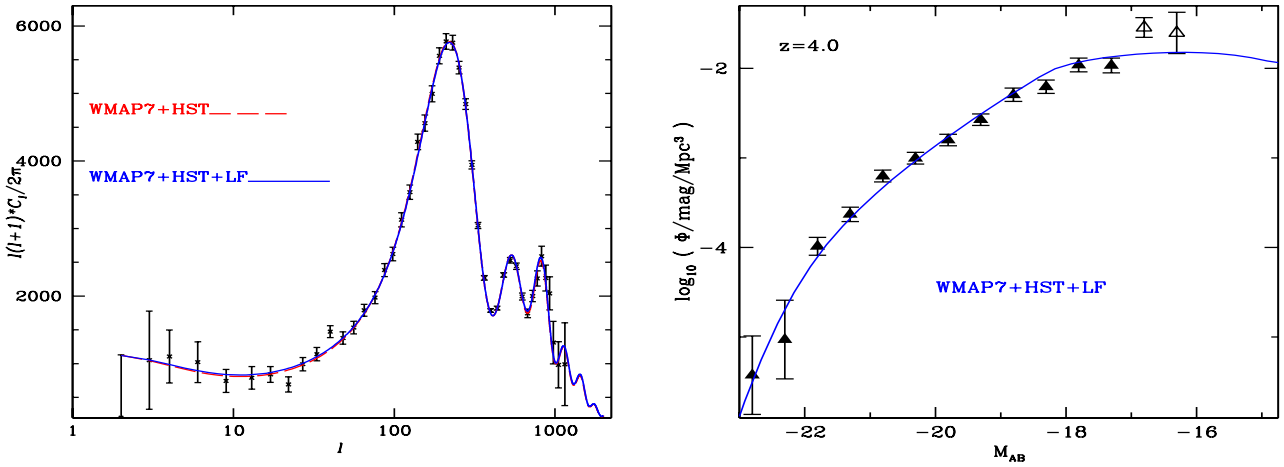

(a)Best fit Cls

(b)Best fit LF at z=4

FIG. 4: The fits to the CMBR TT power spectrum (Cls) (left panel) and the LF at $z = 4$ (right panel) using the best fitted values of cosmological parameters obtained from our MCMC analysis. Solid blue lines are obtained for cosmological parameters corresponding to WMAP7+HST+LF data. The red dashed line in the left panel gives for comparison, Cls for best fitted cosmological parameters based on only WMAP7+HST data.

Σm_ν. We get $\bar{f}_\nu < 0.048$ corresponding to $\Sigma m_\nu \leq 0.55$ eV at the 95% CL. Directly constraining the neutrino mass also leads to a very similar limit, $\Sigma m_\nu < 0.52$ eV at the 95% CL. Thus the limit on the neutrino mass is decreased by a factor of ~ 2 by the addition of the constraints from the $z = 4$ UV LF. The cosmological parameters for these two cases, given respectively in column 3 and 7 of Table II, are very similar. These parameters are also similar to the parameters obtained from WMAP7 alone (column 2 of Table II), except for σ_8, which is increased on including the constraints from the LF data. Note that these limits on Σm_ν, obtained by varying all the cosmological parameters, bear out the naive expectation from the analysis of the Section IV, where we fixed the cosmology.

Next we examined the effect of adding the constraints from the H_0 determination of the HST SHOES (Supernova H0 for the Equation of State) program (which we refer to as HST) ([50]; see also [48]). First WMAP7+HST data alone leads to a tighter neutrino mass limit of $\bar{f}_\nu < 0.052$ (or $\Sigma m_\nu < 0.54$) at 95% CL, consistent with the earlier results of [49]. On adding in the constraint from UV luminosity function data at $z = 4$ this limit is also further decreased. We obtain $\bar{f}_\nu < 0.028$ corresponding to $\Sigma m_\nu \leq 0.31$ eV. (The corresponding cosmological parameters are given in column 4 and 5 of Table II respectively). Again directly constraining the neutrino mass gives a very similar limit, $\Sigma m_\nu < 0.29$ eV at the 95% CL. Therefore, we see that adding in the LF data further decreases the limit on the neutrino mass by another factor of ~ 2. This limit, $\Sigma m_\nu < 0.29$ eV is almost a factor ~ 4 improvement compared to the limit obtained using the WMAP7 data alone. The other cosmological parameters for this case are given in column 8 of Table II and Fig 4 shows the corresponding predicted TT power spectrum of CMBR (Cls) and the LF at $z = 4$ overplotted against the data. In Fig 4 we also plot the Cls corresponding to the parameters which do not include the LF constraint (column 4 of Table II), which shows that Cls for these two cases are almost identical.

All the above neutrino mass limits along with the other cosmological parameters are summarized in Table II. The corresponding 1D marginalized distribution for $\bar{f}_\nu$, from various MCMC analysis, is shown in the top left panel of Fig. 5. The top right 2 panels of Fig. 5 shows 68% and 95% marginalized distributions for H_0 and $\Omega_{DM}h^2$ against $\bar{f}_\nu$, the massive neutrino fraction of the dark matter. The results of directly constraining Σm_ν is shown in the middle panels of Fig. 5. We see also from these figures adding the constraint from the $z = 4$ UV luminosity function significantly improves the constraint on neutrino masses.

In the above analysis we fixed the feedback parameters to $M_{AGN} = 1.8 \times 10^{12} M_\odot$ and $V_u = 95$ km s^{-1}, as described earlier. It is of interest to test the sensitivity of our neutrino mass limits to changes in these values. One way of doing this would be to vary M_{AGN}, V_u and f_*/η as free parameters to obtain the best fit LF and its corresponding likelihood for each step of the MCMC analysis. However, implementing the above procedure in CosmoMC (where the cosmology is also varied) is computationally expensive, and is outside the scope of the present work. Note however that the feedback parameters are expected to depend on physical nature of the feedback mechanisms and not on cosmology. Therefore, as an alternative to varying the feedback parameters within CosmoMC, we adopt our fiducial cosmology and carry out the following procedure. We vary M_{AGN}, V_u and f_*/η in the parameter ranges $10^{11} M_\odot \leq M_{AGN} \leq 5 \times 10^{12} M_\odot$, 85 kms^{-1} $\leq V_u \leq$ 120 kms^{-1} and $0.005 \leq f_*/\eta \leq 1$, to obtain the best fit LF and

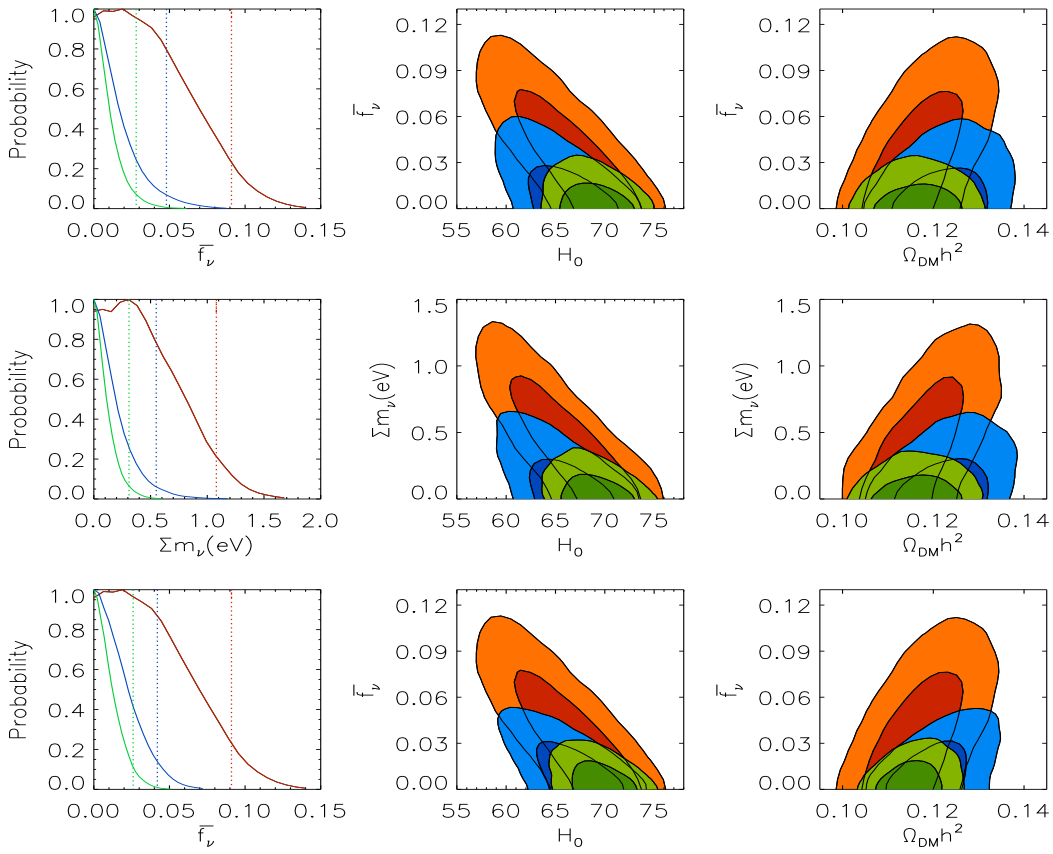

FIG. 5: Various 1D and 2D marginalized distributions from our analysis. The top panel corresponds to our fiducial LF model with feedback parameters $M_{AGN} = 1.8 \times 10^{12} M_\odot$ and $V_u = 95$ km s^{-1}. The middle panel shows plots corresponding to constraining m_ν directly with same feedback parameters as above. The bottom panel is for the LF model with feedback parameters $M_{AGN} = 1.5 \times 10^{12} M_\odot$ and $V_u = 105$ km s^{-1} (model FB). In each row the left panel gives the marginalized 1D distribution for $\bar{f}_\nu$ or m_ν. The vertical dashed lines correspond to 95% confidence levels. The other two panels in each row, show the regions of 68% (dark color) and 95% (light color) confidence levels for H_0 and $\Omega_{DM}h^2$ against $\bar{f}_\nu$ or m_ν. The various contours corresponds to constraints obtained using WMAP7-only (red), WMAP+LF (blue) and WMAP+HST+LF (green) data.

its corresponding χ^2 as a function of Σm_ν. This best fit χ^2 as a function of Σm_ν, obtained after varying all 3 free parameters given above, is shown in Fig. 6. It is clear from Fig. 6 that even after varying the feedback parameters, the global minimum value of χ^2 obtains for the zero neutrino mass case. This global minimum obtains for $V_u = 105$ km s^{-1} and $M_{AGN} = 1.5 \times 10^{12} M_\odot$. The typical 2σ limit is $\Sigma m_\nu = 0.35$ eV, even in this case where all the feedback parameters are varied. This excercise suggests that the uncertainity in the feedback parameters may not have a strong influence on the the upper limit on Σm_ν.

We have repeated our MCMC analysis adopting these best fit values of M_{AGN} and V_u (which we label as model FB). The results of the analysis, adopting the feedback parameters of model FB, are presented in the last 2 columns of Table II and in the bottom panels of Fig. 5. Combining the WMAP7 data and the LF data now leads to a lower limit on the neutrino fraction $\bar{f}_\nu < 0.042$ and a corresponding $\Sigma m_\nu \leq 0.48$ eV. On adding also the constraints from the H_0 determination of the HST SHOES program (together with WMAP7 and UV LF), we get $\bar{f}_\nu < 0.026$ corresponding to $\Sigma m_\nu \leq 0.28$ eV at the 95% CL. We note that these limits on Σm_ν are almost identical to that obtained using the fiducial feedback parameters.

In passing we note that we can also get quantitative measurements of the astrophysical parameter f_*/η at $z = 4$ from our MCMC analysis. These values are given in Table II, while in Fig 7 we plot the 1D marginalized probability distributions (PDF) of f_*/η obtained from the MCMC analysis for a number of models. The red curves are for the fiducial feedback parameters ($M_{AGN} = 1.8 \times 10^{12} M_\odot$ and $V_u = 95$ km s^{-1}) and blue curves are for the model FB

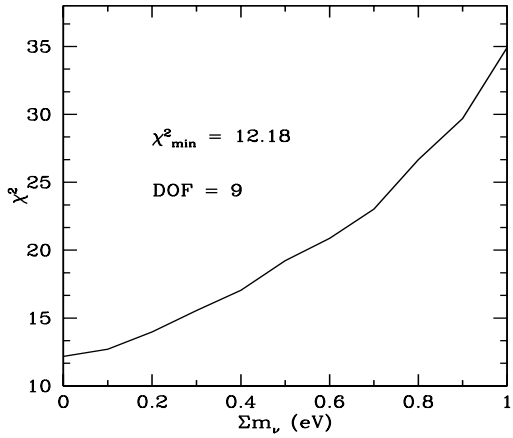

FIG. 6: The Σm_ν vs χ^2 curve for our fiducial cosmology with massive neutrinos. Here we varied M_{AGN}, V_u and f_*/η as free parameters in our model for LF. The solid black curve gives best fit χ^2 as a function of m_ν after marginalizing over all the above three parameters. The number of degrees of freedom is 9.

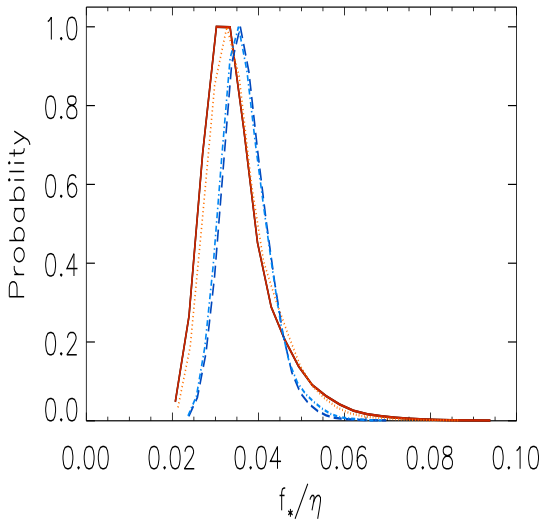

FIG. 7: The 1D marginalized distributions of f_*/η from our analysis using LF at $z = 4$. The solid and dotted (red) curves respectively gives the PDF of f_*/η when one uses WMAP7+LF and WMAP7+HST+LF data with the feedback parameters as in the fiducial LF model. The blue dashed and dashed-dotted curves give the PDF of f_*/η when WMAP7+LF and WMAP7+HST+LF data are used, and for the LF model with feedback parameters FB.

($M_{AGN} = 1.5 \times 10^{12} M_\odot$ and $V_u = 105$ km s^{-1}). In particular the solid (red) and dashed (blue) curves give the PDF of f_*/η when WMAP7 and LF data are combined. The dotted (red) and dashed-dotted (blue) curves are obtained when constraints from WMAP7, HST prior on H_0 and LF are combined. From this figure and Table II, we see that f_*/η is constrained in a narrow range of values, with a mean $f_*/\eta \sim 0.034 - 0.037$. If one adopts a value of $\eta \sim 4$ at $z = 4$ [51], then this corresponds to an $f_* \sim 0.14 - 0.15$. Thus about 15% of baryons need to be converted to stars over several dynamical timescales, to explain the observed UV LF at $z = 4$. This conclusion obtains regardless of the feedback parameters and although we have now explored the full range of cosmological parameters consistent with CMBR, HST and the LF data.

The results of our MCMC analysis in this section shows therefore that fitting the UV LF of high z galaxies can significantly strengthen constraints on the neutrino mass.

VI. CONCLUSIONS

We have proposed here a novel probe of neutrino masses which uses the high redshift UV LF of Lyman break galaxies. In particular, our models constructed in the framework of MDM cosmology, show that the observed shape of the UV LF of high redshift LBGs can be used to constrain the mass of the neutrinos (Σm_ν).

In the presence of massive neutrinos, the matter power spectrum is suppressed below the free-streaming scale. This in turn results in a suppression of the abundance of collapsed halos capable of hosting galaxies at high redshift, compared to a model where $\Sigma m_\nu = 0$. We have studied how this affects the UV LF of LBGs from $z = 3 - 6$. The UV luminosity of a galaxy in our models depends on the parameter f_*/η, where f_* is the total fraction of the baryons converted into stars and $1/\eta$ is the fraction of the total light which comes out of the galaxy after taking into account dust extinction. For a given f_*/η, we find that the number density of galaxies at a given luminosity is suppressed for models with a non-zero neutrino mass compared to the zero neutrino mass case. For example, if $\Sigma m_\nu = 1$ eV this suppression factor is about an order of magnitude at all redshifts, and increases with redshift. In order to best fit the observed UV LF for the models with non zero neutrino mass, the light to mass ratio of each galaxy, governed by the parameter f_*/η has to be correspondingly larger at any redshift. At $z = 6$ for example, we find that f_*/η has to be 6 times larger for a model with $\Sigma m_\nu = 1$ eV compare to the zero neutrino mass case. Moreover, unlike the $\Sigma m_\nu = 0$ case, the best fit f_*/η also increases with z, for models with a non zero Σm_ν. Thus independent constraints on f_*/η, especially at high z, could lead to useful constraints on the neutrino mass.

More importantly, these best fit luminosity functions with a non-zero Σm_ν, obtained by increasing the light to mass ratio of each galaxy (or f_*/η) brings even small mass galaxies, which suffer from various feedback suppression effects, into the observable range. We have shown here that this results in a sensitivity of the LF shape to the neutrino mass. The well measured UV LF of LBGs at $z \sim 4$ is best suited for obtaining quantitative constraints as the data extends over the widest range of luminosities and to much fainter levels than at other redshifts. To obtain quantitative upper limits on Σm_ν, that also explores the full range of cosmological parameters, we have carried out an MCMC analysis using the publically available CosmoMC code [46], after adding also a module which calculates the LF likelihood. The neutrino mass limits obtained here and other cosmological parameters for these models are summarized in Table II. The corresponding 1D and 2D marginalized distribution for $\bar{f}_\nu$ (or Σm_ν), from various MCMC analysis, are shown in Fig. 5.

First, combining the constraints from the WMAP7 data and the UV LF of LBGs at $z \sim 4$, we obtain a constraint on the neutrino fraction $\bar{f}_\nu < 0.048$ and a corresponding limit on sum of neutrino masses, $\Sigma m_\nu < 0.55$ eV at the 95 % CL. Directly constraining Σm_ν in the MCMC analysis leads a similar upper limit $\Sigma m_\nu < 0.52$ eV at the 95 % CL. Thus the neutrino mass limit is not greatly sensitive to whether one specifies a prior on $\bar{f}_\nu$ or Σm_ν. We have also tested the sensitivity of these limits to the feedback parameters. Adopting a different set of feedback parameters (model FB) we get $\bar{f}_\nu < 0.042$ or $\Sigma m_\nu \leq 0.48$ eV at the 95 % CL. Thus the uncertainties related to halo mass (or circular velocity) range over which suppression of star formation due to feedback takes place and exact value of M_{AGN}, do not introduce significant uncertainty in the upper limit on Σm_ν. Our constraints on Σm_ν, obtained by combining the $z = 4$ LF and the WMAP7 data, are a factor of 2 more stringent than constraints that would obtain by using the WMAP7 data by itself.

We have also examined the effect of adding the constraints from the HST prior on H_0. Consistent with the earlier work of [49], we find that WMAP7+HST data alone leads to a tighter neutrino mass limit of $\bar{f}_\nu < 0.052$ (or $\Sigma m_\nu < 0.54$) at 95% CL. This limit is also further decreased to $\bar{f}_\nu < 0.028$ or $\Sigma m_\nu < 0.31$ eV on adding in the constraints from the $z = 4$ LF data. Directly constraining the neutrino mass gives in this case $\Sigma m_\nu < 0.29$ eV at the 95% CL. Adopting model FB for the feedback parameters also gives a similar limit $\bar{f}_\nu < 0.026$ or $\Sigma m_\nu < 0.28$ eV at the 95 % CL. We note that these neutrino mass limits are almost a factor ~ 4 improvement compared to the limit obtained using the WMAP7 data alone.

A summary of the current cosmological and astrophysical constraints on neutrino mass can be found in [52]. Some of the specific results on Σm_ν limits are given by [10–14, 53–56]. The constraints on Σm_ν obtained here adding in the $z \sim 4$ UV LF data to the WMAP7 and HST data, are comparable (or better in several cases) to the above limits. Our work is mainly a demonstrative first step, where we have suggested the utility of the LF of high redshift galaxies to constrain Σm_ν. We have concentrated here on the $z = 4$ UV LF as this is well defined over the widest range of luminosities. Improvements in the LF data, especially at the faint end, and at higher redshifts together with a better understanding of the astrophysics of galaxy formation, will allow us to place more stringent constraints on Σm_ν.

Acknowledgments

CJ thanks CSIR for providing support for this work. We thank Jacob Brandbyge and Toyokazu Sekiguchi for helpful correspondence. We also thank Moumita Aich, Minu Joy, Toyokazu Sekiguchi and Tarun Souradeep for helpful advice

on CosmoMC.

[1] Maltoni M., Schwetz T., Trtola M.A., Valle J.W.F., 2004, New J. Phys.**6**, 122, [arXive:hep-ph/0405172].
[2] Gonzalez-Garcia M. C., Maltoni M., Salvado J., 2010, JHEP, Number 04, 056.
[3] Otten, E. W. & Weinheimer, C. 2008, Rep. Prog. Phys., 71, 086201.
[4] P. Vogel, Nuclear physics aspects of double beta decay, arXiv:0807.2457
[5] Lesgourgues J., Pastor S., 2006, Phys. Rept., **429**, 307.
[6] Hannestad S., 2010, arXiv:1003.4119.
[7] Komatsu E., Smith K. M., Dunkley, J. *et al.*, 2010, ApJS, **192**, 18 (arXiv:astro-ph/1001.4538).
[8] Archidiacono M., Cooray A., Melchiorri A., Pandolfi S., 2010, PRD, **82**, 087302.
[9] Bond, J. R., Szalay, A. S., 1983, ApJ, **274**, 443.
[10] Thomas S. A., Abdalla F. B., Lahav O., 2010, PRL. **105**, 031301.
[11] Mantz A., Allen S. W., Rapetti D., 2009, MNRAS, **406**, 1805.
[12] Seljak U., Slosar A., McDonald P., 2006, JCAP, **10**, 014.
[13] Veil M., Haehnelt M. G., Springel V., 2010, JCAP, **06**, 015.
[14] Tereno I., Schimd C., Uzan J. P., Kilbinger M., Vincent F. H., Fu F., 2009, A&A, **500**,657.
[15] Hu W., Eisenstein D. J., 1998, ApJ, **498**, 497-503.
[16] Eisenstein D. J., Hu W., 1999, ApJ, **511**, 5.
[17] J. Hamann , S. Hannestad, J. Lesgourgues, C. Rampf & Y. Y. Y. Wong, arXiv:astro-ph/1003.3999 (2010).
[18] Dodelson S., Modern Cosmology, 2003, Elsevier Ltd.
[19] Lewis A., Challinor A., Lasenby A., 2000, ApJ, **538**, 473.
[20] W. H. Press and P. Schechter, Astrophys. J. **187** (1974), 425.
[21] Peebles P. J. E., 1980, Large-Scale Structure of the Universe(Princeton: Princeton Univ. Press.)
[22] Padmanabhan T, Subramanian K, 1992, BASI, **20**, 1.
[23] Eke V. R., Cole S., Frenk C. S., 1996, MNRAS **282**, 23.
[24] J. E. Gunn and J. R. Gott, ApJ **176** (1972), 1.
[25] Brandbyge J., Hannestad H., Haugbolle T., Wong Y. Y. Y., 2010, JCAP, **09**, 014.
[26] Marulli, F., Carbone, C., Viel, M., Moscardini, L., Cimatti, A., 2011, arXiv:1103.0278.
[27] Sheth, R. K. Tormen, G. 1999, MNRAS, **308**, 119.
[28] This particular choice of cosmological parameters can be obtained from www.lambda.gsfc.nasa.gov/product/map/dr4/params/lcdm_sz_lens_wmap7.cfm.
[29] S.Sasaki, PASJ, **46** (1994), 427.
[30] Samui S., Subramanian K., Srianand R., 2009, New Astron., **14**, 591 (SSS09).
[31] Samui S., Srianand R., Subramanian K., 2007, MNRAS, **377**, 285 (SSS07).
[32] Chiu W. A., Ostriker J. P., ApJ, 2000, **534**, 507.
[33] Choudhury T. R., Srianand R., 2002, MNRAS, **371**, L55.
[34] Leitherer C., Schaerer D., Goldader J. D. *et al.*, 1999, ApJS, **123**, 3.
[35] Oke J. B., Gunn J. E., 1983, ApJ **266**, 713.
[36] Bromm V., Loeb A., 2002, ApJ, **575**, 111.
[37] Benson A. J., Lacey C. G., Baugh C. M., Cole S., Frenk C. S., 2002, MNRAS, **333**, 156.
[38] Dijkstra M., Haiman Z., Rees M. J., Weinberg D. H., 2004, ApJ, **601**, 666.
[39] Haiman Z., Abel T., & Rees M. J. 2000, ApJ, **534**, 11
[40] Bower R. G., Benson, A. J., Malbon R. et al., 2006, MNRAS, **370**, 645.
[41] Reddy N. A., Steidel C. C., Pettini M., Adelberger K. L., Shapley A. L., Erb D. K., Dickinson M., 2007, ApJ, **175**, 48. (arXiv:0706.4091).
[42] Best P. N., Kaiser C. R., Heckman T. M., Kauffmann G., 2006, MNRAS, **368**, L67.
[43] Fan X., Michael A. S., Robert H. B. *et al.*, 2006, AJ, **132**, 117136.
[44] Beckwith S. V. W., Stiavelli M., Koekemoer A. M., et al., 2006, AJ, **132**, 1729.
[45] Bouwens R. J., Illingworth G. D., Franx M., Ford H., 2007, ApJ **670** (2007),928.
[46] Lewis, A & Bridle, S. 2002, PRD, 66, 103511.
[47] Jarosik N., Bennet C. L., Dunkley J., *et al.*, 2010, arXiv:astro-ph/1001.4744
[48] Freedman W. L., Madore B. F., Gibson B. K., *et al.*, 2001, Astrophys. J. **553**, 47-72.
[49] Sekiguchi T., Ichikawa K., Takahashi T., Greenhill L., 2010, JCAP, **03** 015.
[50] Riess A. G., Macri L., Casetano S., *et al.*, 2009, Astrophys. J. **699** 539-562.
[51] Reddy N. A., Steidel C. C., Pettini M., Adelberger K. L., Shapley A. L., Erb D. K., Dickinson M., 2007, ApJ, **175**, 48.
[52] Abazajian K. N. et al., 2011, [arXiv:1103.5083].
[53] Reid B. A., Verde L., Jimenez R., Mena O., 2010, JCAP, **01**, 3.
[54] Swanson M E C., Percival W. J., Lahav O., 2010, [arXiv:1006.2825].
[55] Li H., Liu J., Xia J. Q. *et al*, 2009, PhLB, **675**, 164.
[56] Ichiki K., Takada M., Takahashi T., PRD, **79**, 023520.